A temperature-insensitive polarization filter and a neotype sensor based on a hybrid-circular-hole microstructured optical fiber*

GUO Jun-qi (郭俊启)**, ZHOU Min** (周敏)**, LU Yong-le** (路永乐)**, DI Ke** (邸克)**, HAN Jun-jian** (韩军健)**, TANG Chuan** (唐川)**, XU Xiao-hu** (徐小虎)**, and LIU Yu** (刘宇)**

Chongqing Municipal Key Laboratory of Photoelectronic Information Sensing and Transmitting Technology, Chongqing University of Posts and Telecommunications, Chongqing 400065, China

(Received 20 April 2018; Revised 9 May 2018)

A temperature-insensitive polarization filter and a neotype sensor based on a hybrid-circular-hole microstructured optical fiber (MOF) are proposed. Numerical investigations demonstrate that the *x* polarized component of silica core mode can couple to the cladding mode in the researched wavelength, while the *y* polarized component would not. Furthermore, the resonant region can be controlled by changing the diameters or coordinates of the air holes, and the MOF has good performance on stability of temperature. Moreover, the hybrid-circular-hole structure is propitious to selectively integrate different functional materials. Two different materials are integrated into this proposed MOF, the application of the Sagnac interferometer in temperature sensing is studied, and two groups of dips would be observed in the transmission spectra, which have different temperature sensitivities. Therefore, the proposed MOF can be used as a flexible temperature-insensitive polarization filter or potentially applied to a two-parameter sensor.

Document code: A **Article ID:** 1673-1905(2018)04-0280-6

DOI https://doi.org/10.1007/s11801-018-8060-7

In recent years, plenty of microstructured optical fiber (MOF)[1-4] polarization filters have been studied and designed, which have different characteristics. Mohamed et al[5] designed a novel ultra-high tunable liquid crystal polarization filter by infiltrating nematic liquid crystal (NLC) and metal wires into cladding air holes, and Xue et al[6] studied the polarization filter characteristics of a gold-coated and liquid-filled photonic crystal fiber. The resonance strength of both polarization filters can achieve more than 50 dB/cm. But the liquid is susceptible to temperature, which would make the polarization filters unstable in variable temperature environment.

Although the fiber polarization filters based on liquid infiltration in the literatures have good performance on resonance characteristics, the high temperature sensitivity of the polarization filter created in conventional single-mode fiber is a disadvantage for its application in optical fiber communications. Wang et al[7] have designed a polarized filtering photonic-crystal fiber by coating the gold on the inner walls of the air hole. Liu et al[8] have proposed a broadband single-polarization photonic crystal fiber polarized filter based on surface plasmon resonance. Both of the two polarization filters have good performance on stability of temperature and simple structure. However, the polarization filters reported above all need to integrate some materials, which means the complex manufacturing processes. What's more, it's difficult to reintegrate more functional materials into these fibers and maintain resonant coupling.

In this paper, a temperature-insensitive polarization filter and a neotype sensor based on a hybrid-circular-hole MOF are proposed, the air holes of which are arranged in a regular hexagonal pattern. The resonant region and the impact of structural parameters of the MOF and temperature on the location of strongest resonant point (SRP)[9] are studied. Two different functional materials are integrated into this proposed MOF and applied to the Sagnac interferometer. The temperature sensitivity based on the Sagnac interferometer is analyzed, and two groups of dips would be observed in the transmission spectra, which have different temperature sensitivities.

The schematic of the hybrid-circular-hole MOF is shown in Fig.1. There are five rings of air holes arranged in a regular hexagonal pattern with two larger holes beside fiber core along *x* axis, the diameters of the smallest hole and large hole are d_1=2.1 μm and d_2=5.6 μm, respectively, the distance between the adjacent smallest air

* This work has been supported by the National Natural Science Foundation of China (Nos.61705027 and 11704053), the Innovation Leader Talent Project of Chongqing Science and Technology (No.CSTCCXLJR20171160), and the Basic Research Project of Chongqing Science and Technology Commission (Nos.KJZH17115, Cstc2017csmsA40017, KJ1704091, KJ1704104 and KJ1704106).

** E-mail: liuyu@cqupt.edu.cn

holes is 4.9 μm and the coordinates of the large hole are (X_2=4.9 μm, Y_2=0 μm) in the first quadrant. There are three special groups of air holes located in the first ring, second ring and third ring, respectively, which are symmetrical about the axis. In the first quadrant, the diameter and coordinates of hole 5 in the first ring are d_5=3.0 μm and (X_5=2.0 μm, Y_5=4.6 μm), those of hole 4 in the second ring are d_4=3.6 μm and (X_4=2.28 μm, Y_4=8.487 μm), and those of hole 3 in the third ring are d_3=4.0 μm and (X_3=2.45 μm, Y_3=12.73 μm). The refractive indices of the air hole and the background silica are set as n_1=1 and n_2=1.444, respectively.

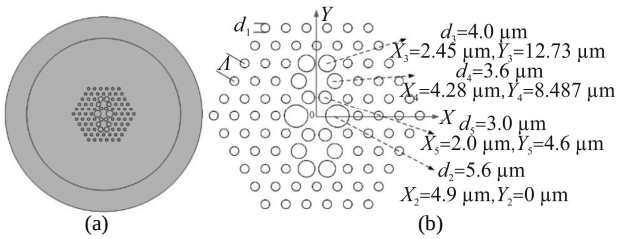

Fig.1 (a) Schematic diagram of the hybrid-circular-hole microstructured optical fiber; (b) Arrangement and parameters of air holes in the fiber

Firstly, we theoretically calculate the hybrid-circular-hole MOF by full-vector finite element method (FEM). The proposed structure is axisymmetric, and we can calculate a quarter of this fiber to reduce the computation. We use COMSOL software to calculate the effective refractive indices of modes ranging in 600—1 700 nm, which is the wavelength range that can be measured in the simulation. It can be seen from Fig.2(b) that the difference of two modes achieves the minimum at the wavelength of 986 nm and we call the wavelength as SRP. In Fig.2(c), the arrows represent the polarization directions. At shorter wavelength, the phase matching condition between the silica core mode and the cladding mode is not obtained, and the two modes will not couple and keep independent transmission. With the increase of the wavelength, the phase matching of two modes increases gradually, and the two modes will experience a strong and complex coupling process in the resonant region, where a fraction of optical energy transfers from the silica core mode to the cladding mode. At longer wavelength, the phase mismatch increases gradually, where the mode coupling gradually weakens, and the mode fields of two modes exchange and keep independent transmission. The dispersion curves are close in the center of the resonant region, where the effective refractive index differences between the silica core mode and the cladding mode are small, which means that the phase matching condition is easy to meet and the mode coupling is the strongest. Deviating from the center of the resonant region, the phase mismatch will be increased and the resonance will become weaker.

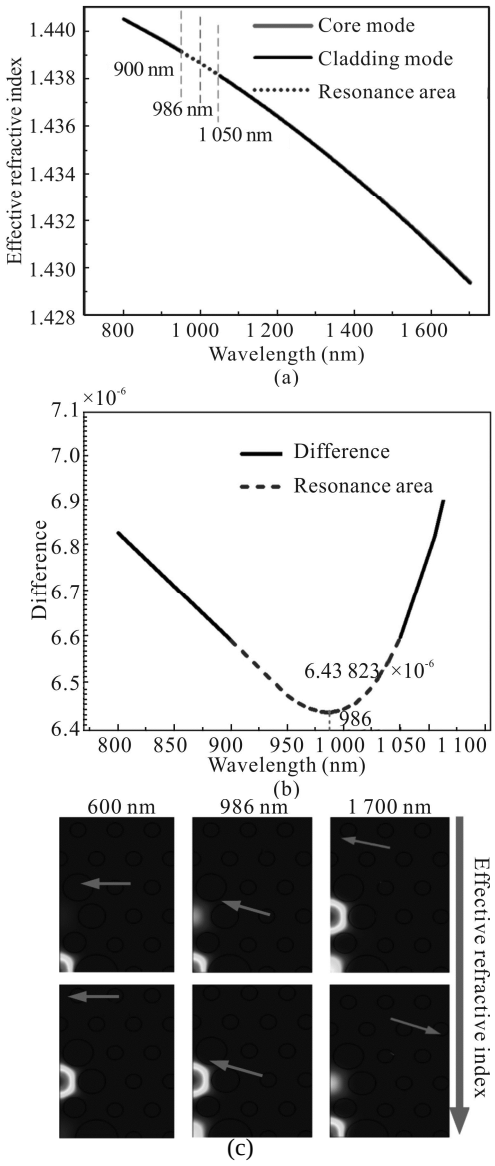

Fig.2 (a) The modal effective indices of the *x*-polarization silica core mode n_{1x} and the cladding mode n_{2x}; (b) The effective refractive index difference between the silica core mode and the cladding mode; (c) The mode fields of the two modes at different wavelengths

As we can see from Fig.3, in the researched wavelength range, the phase matching condition between the silica core mode and the cladding mode is not satisfied, and there is no coupling or resonance energy transfer between the silica core mode and the cladding mode, where the two modes would keep independent transmission.

Within the wavelength range that can be measured in the simulation, only *x*-polarization silica core mode can be coupled with the cladding mode, and the optical energy transfer from silica core mode to mode of cladding occurs only for *x*-polarized component, while *y*-polarization silica core mode does not meet the phase matching condition and can be approximately regarded as remaining inside the fiber core. Therefore, the

proposed MOF has the characteristic of polarization filtering in the resonant region.

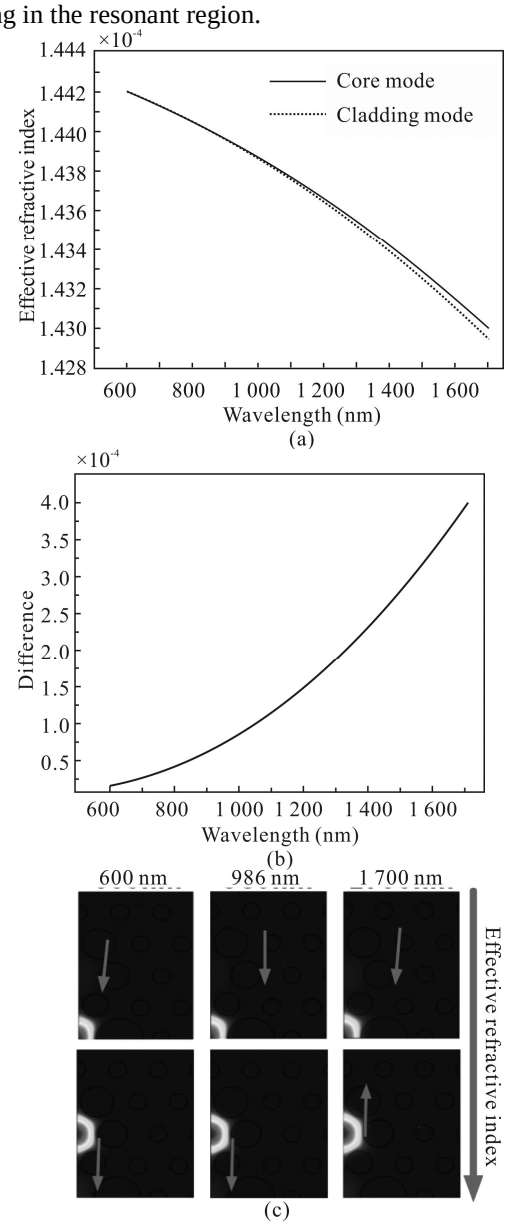

Fig.3 (a) The modal effective indices of the *y*-polarization silica core mode n_{1y} and the cladding mode n_{2y}; (b) The effective refractive index difference between the silica core mode and the cladding mode; (c) The mode fields of the two modes at different wavelengths

To further analyze the coupling processes, we introduce the coupling length. When light couples from the fiber core to the cladding, the coupling length can be expressed as

$$L_c = \frac{\lambda}{2\Delta n} \quad , \tag{1}$$

where Δn is the difference of the refractive indices between the core mode and cladding mode, and λ is the operation wavelength.

According to Eq.(1), the coupling length of *x*-polarization silica core mode at the wavelength of SRP λ=986 nm is 0.076 6 m. When the length of fiber is $L_f=2NL_c+1$ (where N can be any integer), the coupling from the fiber core to the cladding can reach an optimum.

The hole-to-hole distance and the hole diameters of proposed MOF are not identical, and studies show that changing the hole-to-hole distance or the hole diameters would affect the location of the resonant region, especially the air holes around the silica core mode and the cladding mode. Since the MOF is symmetrical about the axis, we can use the air holes located in the first quadrant to represent the corresponding types of air holes to analyze the effect of the air hole diameters and coordinate values on the resonant region. Figs.4—6 show the wavelength change curves of SRP with different hole diameters, X values and Y values.

Fig.4(a) shows the relationship between the diameter of air hole 3 and the wavelength of SRP with five different hole diameters of 3.996 μm, 3.998 μm, 4.0 μm, 4.002 μm and 4.004 μm, respectively, and X_3=2.45 μm, Y_3=12.73 μm. We can see that the wavelength of SRP experiences red-shift with the increase of the hole diameter, and the effective refractive index difference between the silica core mode and the cladding mode is increasing with increasing diameter. When the diameter and the Y value of hole 3 are d_3=4.0 μm and Y_3=12.73 μm, the location changing process of SRP with different X_3 values of hole 3 is shown in Fig.4(b), and the X_3 values are 2.448 μm, 2.449 μm, 2.45 μm, 2.451 μm and 2.452 μm, respectively. The wavelength of SRP will be blue-shift with the increase of the X_3 value, and the modal effective refractive index difference will be reduced. Fig.4(c) shows the relationship between the Y value of air hole 3 and the wavelength of SRP with different Y_3 values of 12.728 56 μm, 12.729 56 μm, 12.730 56 μm, 12.731 56 μm and 12.732 56 μm, respectively, and the air hole diameter is d_3=4.0 μm under the same X value of X_3=12.73 μm. With the increase of Y_3 value, the location of SRP and the difference of two effective refractive indices will be decreased. As seen from Fig.4, the wavelength of SRP will be red-shift with the increase of diameter, while the wavelength of SRP will be blue-shift with the increase of X_3 and Y_3 values. The variation of X_3 has less influence on the location of SRP while the hole diameter and Y_3 affect the location of SRP strongly.

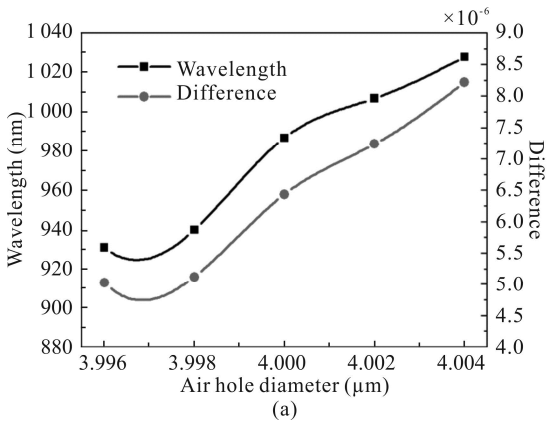

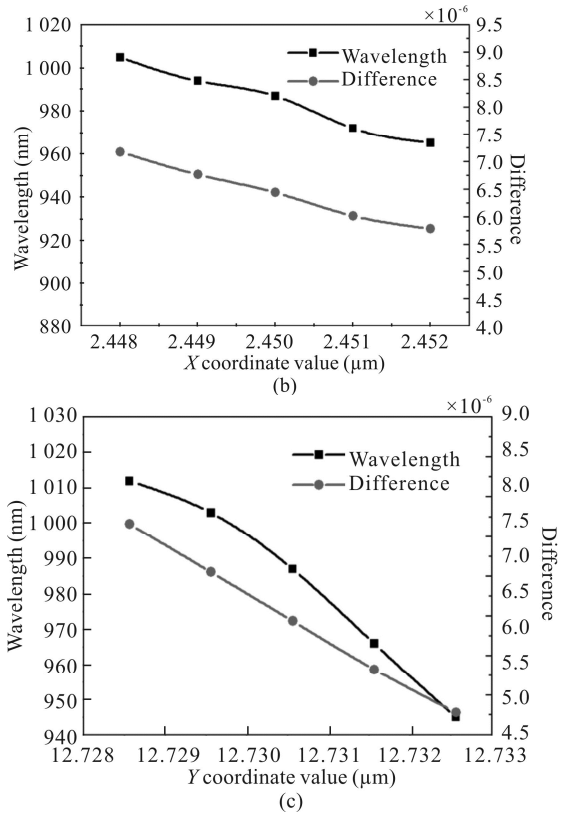

Fig.4 (a) The wavelength change curves of SRP with different diameters of hole 3; (b) The location change curves of SRP at different X_3 values; (c) The wavelength change curves of SRP at different Y_3 values

As shown in Fig.5(a), while the diameter of hole 4 is changed from 3.596 μm to 3.604 μm, the wavelength of SRP is increased from 931 nm to 1 014 nm, and the effective refractive index difference of two modes is also increased from $5.026\,34\times10^{-6}$ to $9.489\,79\times10^{-6}$. From Fig.5, the location of SRP will be red-shift with the increase of diameter, while the location of SRP will be blue-shift with the increase of X_4. The changes of Y_4 have little effect on the location of SRP, while the hole diameter and Y_4 affect the location of SRP strongly.

We can see from Fig.6 that the location of SRP will be red-shift, and the effective refractive index difference between silica core mode and the cladding mode will be increased with the increase of Y_5, while the diameter and X value of hole 5 have a little influence on the location of SRP.

From the analysis above, we can regulate the location of resonant region by changing the hole-to-hole distance or the hole diameter of the proposed MOF. Therefore, a flexible polarization filter could be designed.

Since the proposed MOF is pure silica fiber, we can theoretically simulate the effect of temperature with the thermal coefficient of a pure silica substrate of 8×10^{-6} °C^{-1}. Fig.7 shows the wavelength change curves of SRP with different temperatures of 15 °C, 25 °C, 35 °C, 45 °C and 55 °C, respectively. We can see that the wavelength of SRP at all five temperatures is 986 nm, which is hardly affected by temperature.

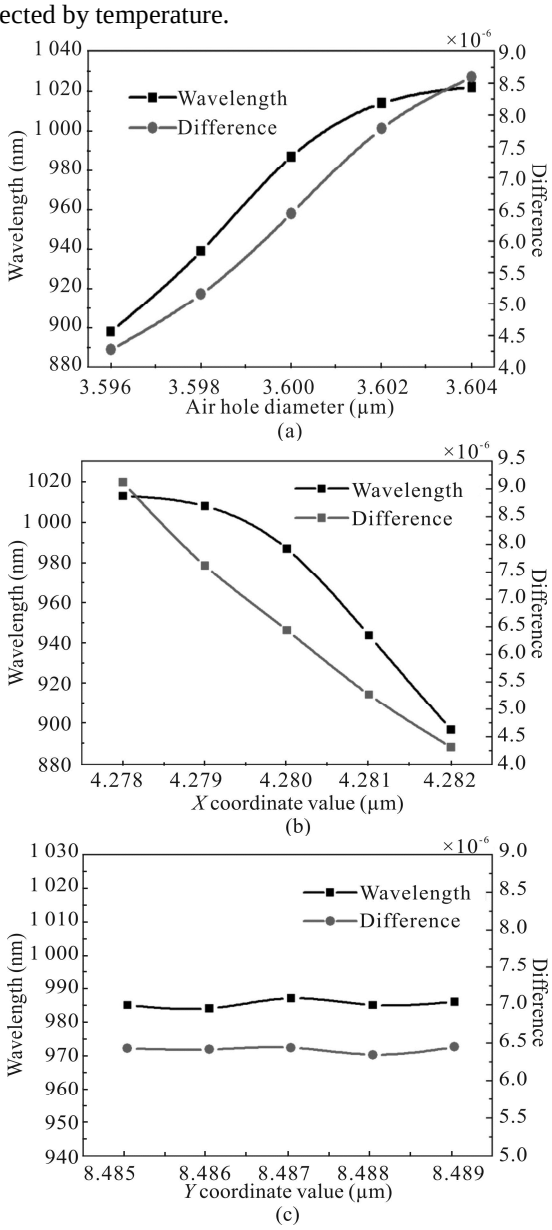

Fig.5 (a) The wavelength change curves of SRP with different diameters of hole 4; (b) The location change curves of SRP at different X_4 values; (c) The wavelength change curves of SRP at different Y_4 values

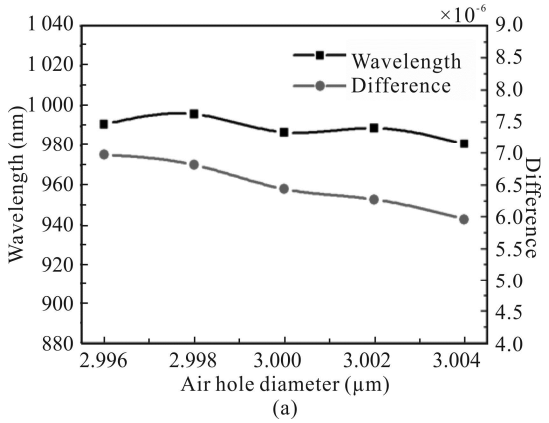

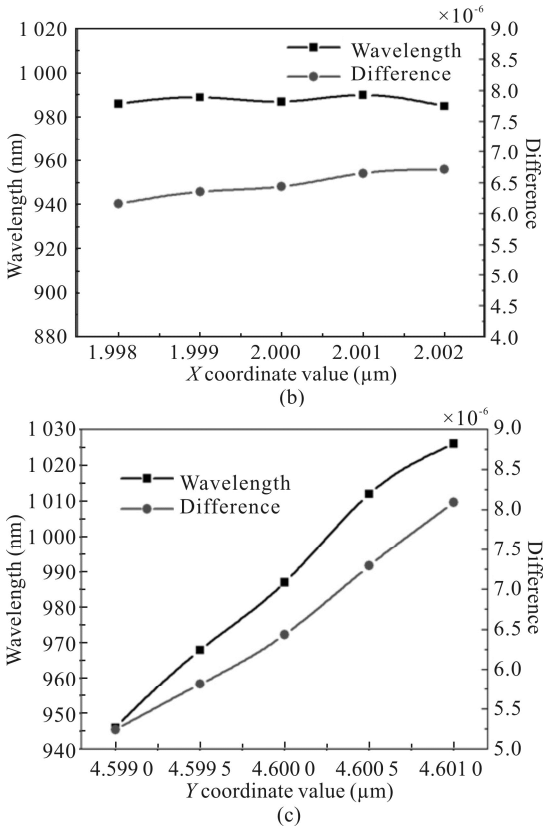

Fig.6 (a) The wavelength change curves of SRP with different diameters of hole 5; (b) The location change curves of SRP at different X_5 values; (c) The wavelength change curves of SRP at different Y_5 values

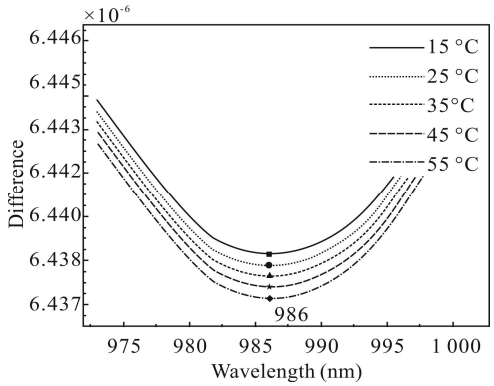

Fig.7 The wavelength change curves of SRP with different temperatures

For the thermal coefficient of a pure silica substrate is 8×10^{-6} °C^{-1}, the temperature has a little influence on the length of fiber. As we can see from Fig.7, at 15 °C, 25 °C, 35 °C, 45 °C and 55 °C, the differences of the refractive indices Δn at the wavelength of SRP λ=986 nm are $6.438\,6\times10^{-6}$, $6.438\,2\times10^{-6}$, $6.437\,8\times10^{-6}$, $6.437\,4\times10^{-6}$ and $6.437\,0\times10^{-6}$, respectively. According to Eq.(1), we can calculate the coupling length at all five temperatures is about 0.076 6 m, so the coupling length can be hardly affected by temperature. Hence the MOF has good performance on stability of temperature, which can work stably in variable temperature environment.

We will integrate two different functional materials into the MOF and apply it to the Sagnac interferometer. The cross section of the MOF filled by liquid is shown in Fig.8(a), where the smallest holes and largest holes are infiltrated with the liquid which possesses a refractive index of 1.3 at 25 °C, and the other holes are filled by the liquid with a refractive index of 1.32 at 25 °C. The thermal-optic coefficients of two materials are both −0.000 404/°C, and the filling fiber length L is set to be 5 cm. For the Sagnac interferometer, there are two light beams divided by 3 dB couple, they go through the polarization maintaining fiber clockwise and counter-clockwise, respectively, which causes a phase difference and results in interference fringes[10,11], and the structure of Sagnac interferometer is shown in Fig.8(b).

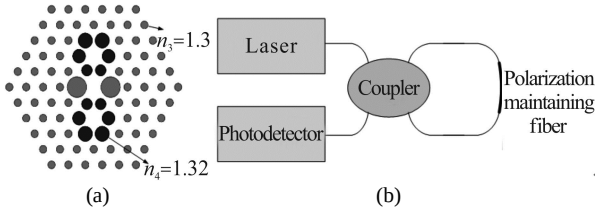

Fig.8 (a) Cross section of the MOF filled by liquid; (b) Structure of Sagnac interferometer

The resonant coupling still exists between the core mode and the cladding mode of the liquid filled fiber, so we would observe two groups of dips in the transmission spectra. One of the dips comes from the coupling between the core mode and the cladding mode, and the other results from interference. For the MOF is a pure silica fiber, which has extremely tiny thermal coefficient, the temperature has a little effect on the length of fiber and the birefringence. When we ignore the thermal coefficient of the pure silica substrate, Fig.9 shows the drift tendencies of the wavelength of SRP at 15 °C, 20 °C, 25 °C, 30 °C, 35 °C, 40 °C and 45 °C. With the increase of the temperature, the wavelength of SRP experiences red shift. As shown in Fig.9, the relationship between the wavelength of SRP and the temperature keeps a good linearity, and the temperature tuning velocity of the wavelength of SRP is about 3.12 nm/°C.

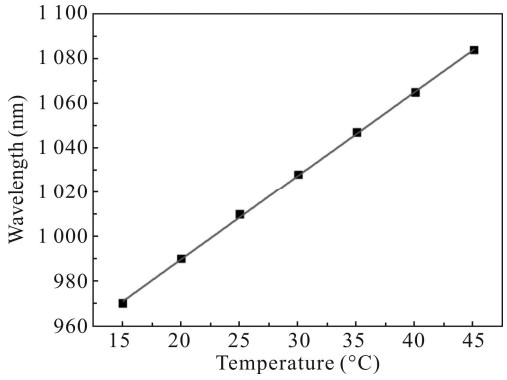

Fig.9 The wavelengths of SRP at different temperatures

For the Sagnac interferometer, the transmission interference spectrum formula can be expressed as

$$T_t(\lambda) = \frac{1-\cos(\delta)}{2}, \quad (2)$$

where λ is the wavelength, and δ is the phase difference caused by the birefringent fiber, which can be defined as

$$\delta = 2\pi LB(\lambda)/\lambda, \quad (3)$$

where B is the birefringence of the core mode, which can be expressed as

$$B(\lambda) = \mathrm{Re}\left|n_{\mathrm{eff}}^{\ y}(\lambda) - n_{\mathrm{eff}}^{\ x}(\lambda)\right|, \quad (4)$$

where $n_{\mathrm{eff}}^{\ y}(\lambda)$ and $n_{\mathrm{eff}}^{\ x}(\lambda)$ are the effective refractive indices of the *y*-polarization core mode and *x*-polarization core mode, respectively.

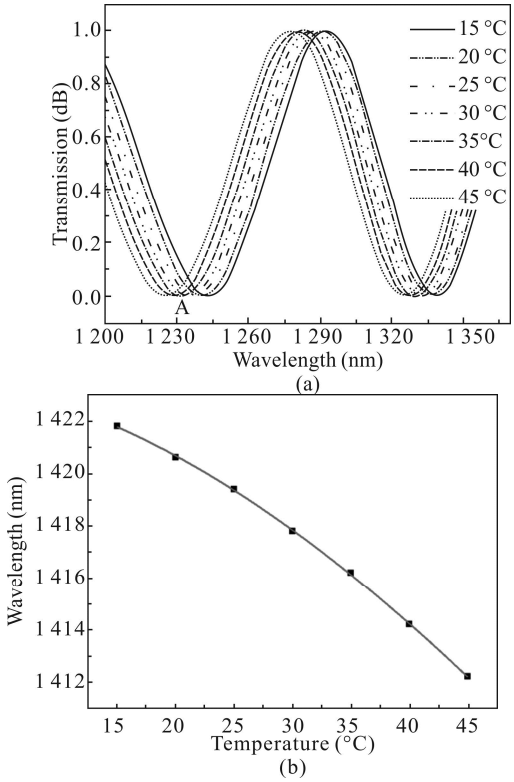

Fig.10 (a) Transmission spectra of Sagnac interferometer at different temperatures; (b) The tendency of the interference dip wavelength with temperature

The birefringence values of this liquid filled fiber at different temperatures are calculated by the FEM. According to Eq.(2), the transmission spectra at different temperatures are shown in Fig.10(a). With temperature rising, all the dips experience blue shift. Fig.10(b) shows the drift tendencies of dip A at 15 °C, 20 °C, 25 °C, 30 °C, 35 °C, 40 °C and 45 °C. As the temperature increases, the drift velocity is getting faster. The sensitivity at T=15 °C is about S=−0.483 nm/°C, while the sensitivity is about S=−0.693 nm/°C at T=45 °C. Both of these temperature sensitivities of dip A are different from that of the wavelength of SRP. Based on the above results, the proposed MOF has a potential to be a temperature sensor after being filled with functional materials.

In this paper, we present a hybrid-circular-hole MOF, and numerically investigate the mode coupling process and the effect of air hole diameters, the coordinate values and temperature on resonant region. We find that only *x* polarized component of silica core mode can couple to the cladding mode within the measured wavelength. We can control the resonant region by flexibly changing the diameter or hole-to-hole distance of air holes, so a flexible filter can be designed. The resonant region has a little sensitivity to temperature, so the fiber can work stably in variable temperature environment. When we integrate two functional materials into this fiber, the wavelengths of SRP and resonant dip have tuning velocities of temperature at about 3.12 nm/°C and −0.5 nm/°C, respectively. Therefore, this proposed MOF can be used as a flexible polarization filter and a two-parameter sensor or other devices.

References

[1] Favero F. C., Becker M., Spittel R., Rothhardt M., Kobelke J. and Bartelt H., Photonic Sensors **3**, 208 (2013).

[2] Xu Y. and Bao X., Canadian Journal of Physics **999**, 1 (2017).

[3] Islam I., Paul B. K., Ahmed K., Hasan R., Chowdhury S., Islam S., Sen S., Bahar A. N. and Asaduzzaman S., Sensing and Bio-sensing Research **14**, 30 (2017).

[4] Zi J., Li S., Chen H., Li J. and Li H., Plasmonics **11**, 65 (2016).

[5] Hameed M. F. O., Heikal A. M., Younis B. M., Abdelrazzak M. and Obayya S. S. A., Optics Express **23**, 7007 (2015).

[6] Xue J., Li S., Xiao Y., Qin W., Xin X. and Zhu X., Optics Express **21**, 13733 (2013).

[7] Wang G., Li S., An G., Wang X., Zhao Y. and Zhang W., Applied Optics **54**, 8817 (2015).

[8] Liu Q., Li S., Li H., Zi J., Zhang W., Fan Z., An G. and Bao Y., Plasmonics **10**, 931 (2015).

[9] Guo J., Liu Y. G., Wang Z., Han T., Huang W. and Luo M., Optics Express **22**, 7607 (2014).

[10] Xin Y., Dong X., Meng Q., Qi F. and Zhao C. L., Sensors and Actuators A: Physical **193**, 182 (2013).

[11] Reyes-Vera E., Cordeiro C. M. and Torres P., Applied Optics **56**, 156 (2017).